Supporting Information for

Geometric and Electronic Engineering of Mn doped $Cu(OH)_2$ Hexagonal Nanorings for Superior Oxygen Evolution Reaction Electrocatalysis

Hui Xu, Hongyuan Shang , Junwei Di *, and Yukou Du *

College of Chemistry, Chemical Engineering and Materials Science, Soochow University, Suzhou 215123, PR China

** Corresponding authors: Tel: 86-512-65880089, Fax: 86-512-65880089;*

E-mail: djw@suda.edu.cn (J. Di); duyk@suda.edu.cn (Y. Du)

Supplementary Method

Experimental Section

Synthesis of $Mn(OH)_2$ nanoplates: Synthesis of $Mn(OH)_2$ nanoplates was based on the reported method with appropriate modification.[1] 158 mg of $KMnO_4$ was dissolved in 20 mL deionized water at room temperature and 2.5 mL of hydrazine hydrate (N_2H_4, 80%) was added into the above solution slowly, and then sonicating for 1 min. The obtained suspension was transferred into a 50 mL Teflon-lined stainless steel autoclave, sealed, and maintained at 180 °C for 12 h and then air-cooled to room temperature. The product was centrifuged and thoroughly washed with ethanol/water for several times, and then dispersed in 10 mL deionized water for further use.

Synthesis of Mn doped $Cu(OH)_2$ hexagonal nanorings: 2 mL of $Mn(OH)_2$ nanoplates precursor was re-dispersed into 10 mL of 0.05 M $CuCl_2 \cdot 2H_2O$ solution and stirred at 25°C for 12 h. The green precipitate was centrifuged and washed with water for several times before dried. For comparison, we have also varied the addition of $Mn(OH)_2$ nanoplates precursor to 1 mL and 4 mL, and the products were denoted as Mn doped $Cu(OH)_2$-1 mL and Mn doped $Cu(OH)_2$-4 mL, respectively.

Synthesis of $Cu(OH)_2$: The synthesis of $Cu(OH)_2$ is also similar to the Mn doped $Cu(OH)_2$ hexagonal nanorings but changing the addition of 2 mL of $Mn(OH)_2$ nanoplates to NaOH solution. The products were collected by centrifugation and washed with water and ethanol three times, respectively. The obtained product was ready for further processing and characterization.

Materials characterizations: The transmission electron microscopy (TEM) images were performed utilizing FEI Tecnai T20 microscope (200 kV), and high-resolution TEM (HRTEM) images and element mapping analyses results were obtained on an FEI Tecnai F30 microscope (300 kV) with an Energy Dispersive Spectrometer (EDX). Scanning electron microscopy (SEM) images were taken on a Merlin Compact scanning electron microscope. Powder X-ray diffraction (PXRD) patterns were obtained using a Rigaku X-ray diffractometer equipped with Cu-Kα radiation at 40 kV and 100 mA, respectively. XPS measurements were performed on Imaging Photoelectron Spectrometer (Axis Ultra DLD, Kratos Analytical Ltd.) using monochromatized Al Kα anode (Al Ka, hv=1486.7 eV). All the collected spectra were calibrated with contaminated C 1s peak at 284.8 eV. The EPR measurements were performed on a Bruker Elexsys E580 X-band

pulsed-EPR spectrometer.

Electrode fabrication: The sample ink was prepared by mixing the catalyst (1 mg), propanol, and Nafion (0.5 wt%, 20 μL) followed by sonication for 30 min. Then the ink was drop-casted onto a Ni foam (2 cm^2) and used as the working electrode for measurements. The catalyst loading was determined to be ~0.5 mg cm^{-2}. The electrochemical measurements were conducted on a standard three electrode system with a CHI 760E electrochemistry workstation using 1.0 M KOH solution as electrolyte. A three-electrode electrochemical cell was employed with Ag/AgCl as the reference electrode (3 M KCl), as-prepared sample modified glassy carbon as the working electrode, and carbon rod as the counter electrode. Before the electrocatalytic activity tests, all catalysts were conditioned by potential cycling over 60 cycles at a scan rate of 50 mV s^{-1} in 1 M KOH. Linear sweep voltammetry (LSV) curves were obtained by sweeping the potential from 1 to 1.7 V (vs. RHE) at room temperature at a sweep rate of 5 mV s^{-1}. The electrochemical impedance spectra (EIS) measurement was performed in the same configuration at room temperature over a frequency range from 0.1 Hz to 1000 kHz. Long-term stability is evaluated by the LSV after continuous cyclic voltammetry (CV) measurement for 3000 cycles and prolonged chronopotentiometry test at the current density of 10 mA cm^{-2} for long period.

Calculation of ECSA: The calculation of the electrochemical surface areas (ECSA) are based on the measured double layer capacitance of the electrode in 1.0 M KOH according to previous published report. Briefly, a potential range where no apparent Faradaic process happened was determined firstly using the static cyclic voltammetry (CV). The charging current i_c was measured from the CVs at different scan rates. The relation between i_c, the scan rate (ν) and the double layer capacitance (C_{DL}) was given in eq 1. Thus the C_{DL} is then calculated according to: C_{DL}=d (Δj (0 V vs. RHE))/2dv.

$$i_c = \nu C_{DL} \qquad (1)$$

Therefore, the slope of i_c as a function of ν will give a straight line with the slope equal to C_{DL}.

$$ECSA = C_{DL}/ C_S \qquad (2)$$

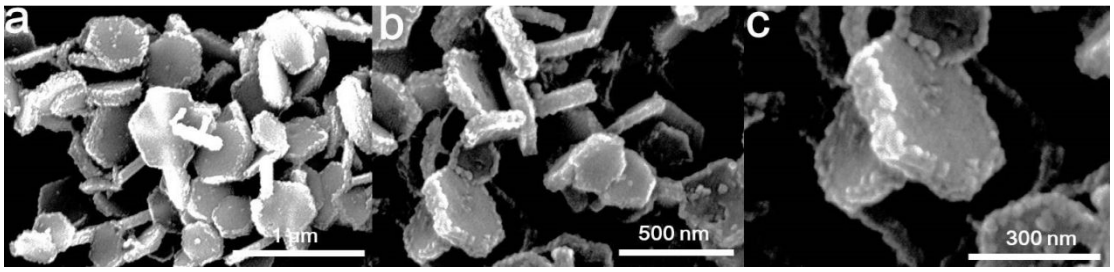

Figure S1. (a-c) Representative SEM images of $Mn(OH)_2$ nanoplates with different magnifications.

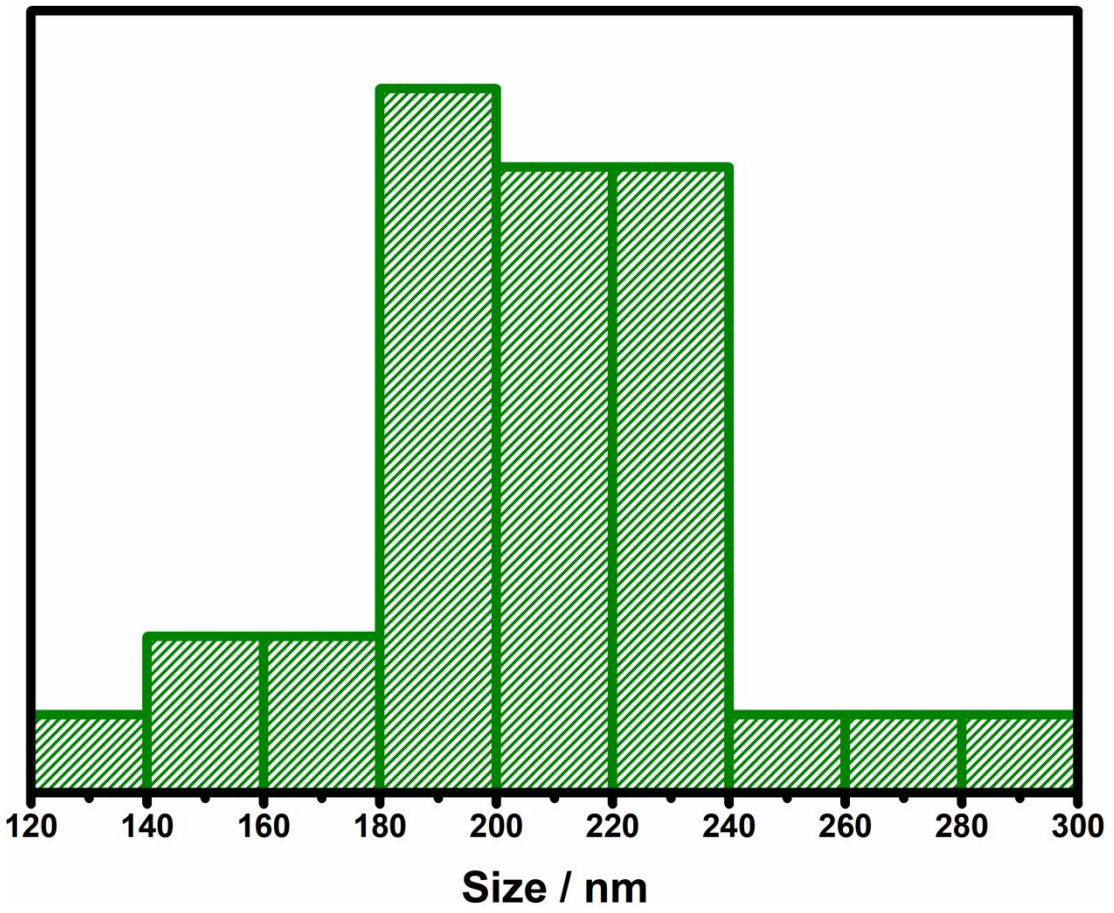

Figure S2. Size distribution of $Mn(OH)_2$ nanoplates.

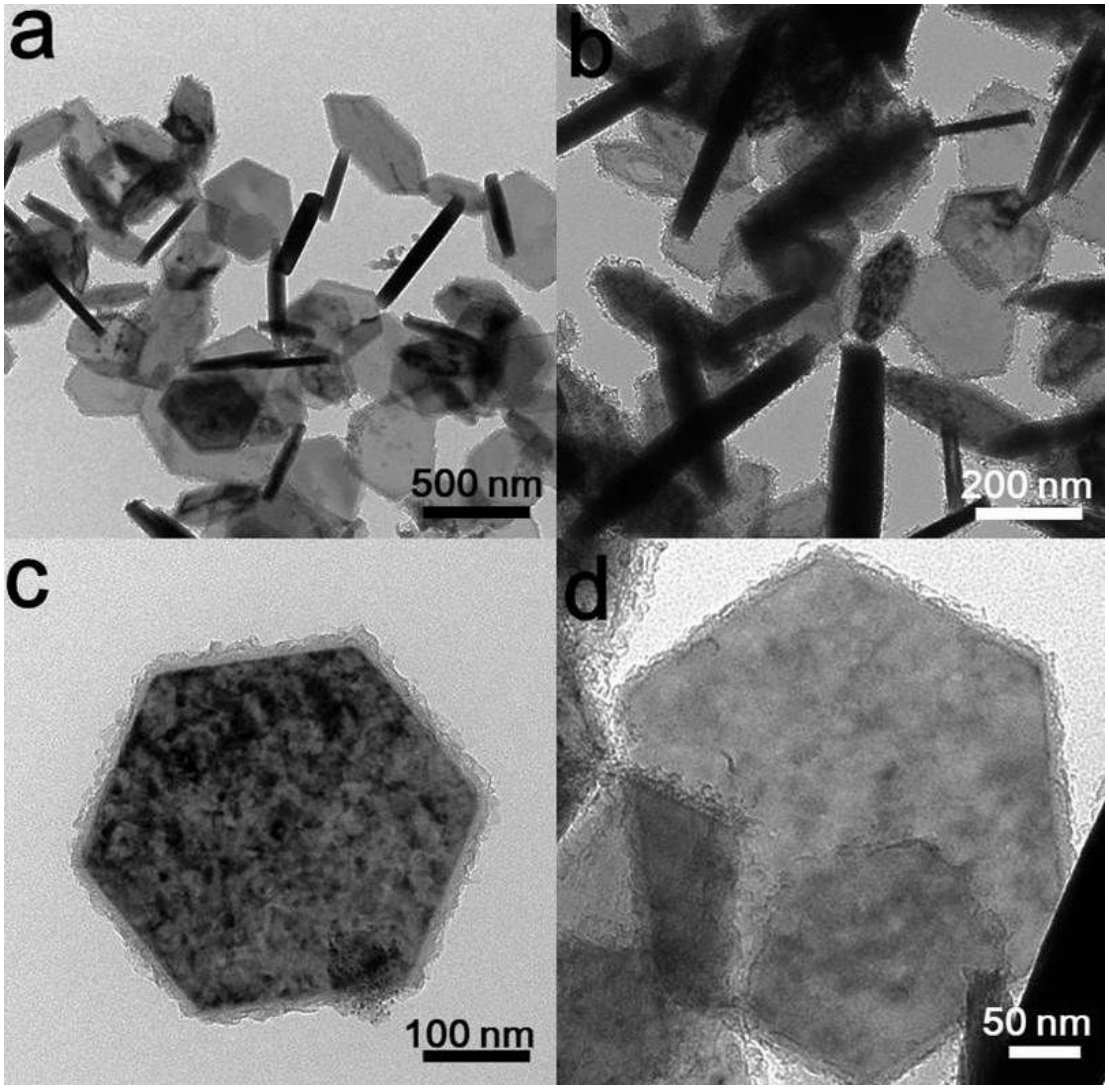

Figure S3. (a-d) Representative TEM images of $Mn(OH)_2$ nanoplates.

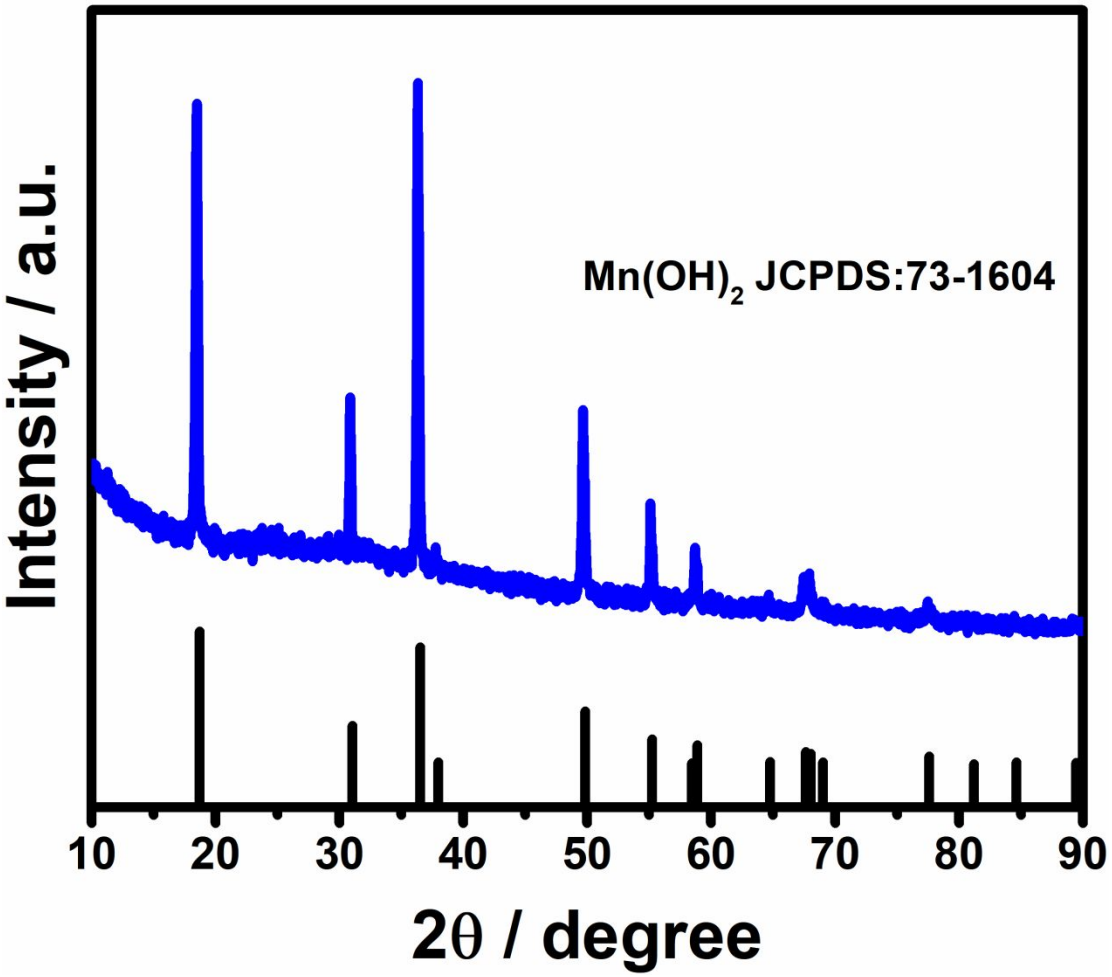

Figure S4. XRD pattern of $Mn(OH)_2$ nanoplates.

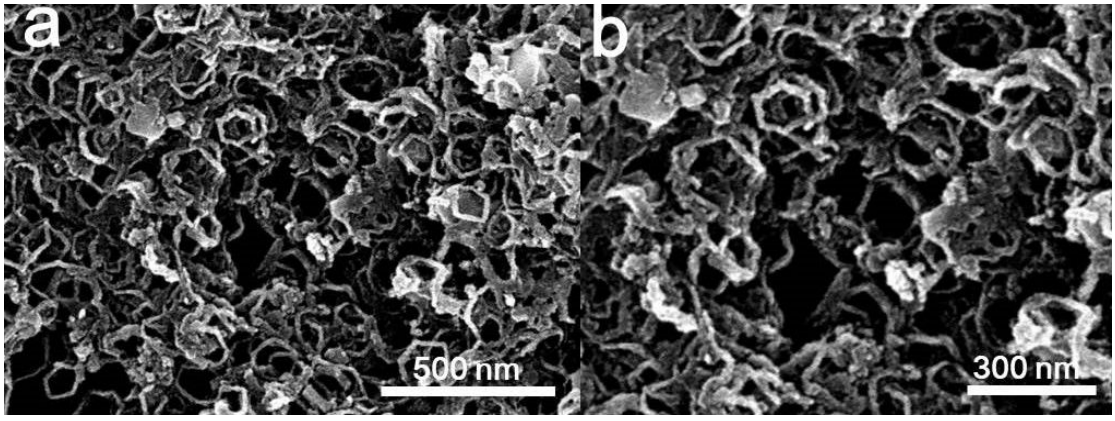

Figure S5. Representative SEM images of (a and b) Mn doped $Cu(OH)_2$ hexagonal nanorings with different magnifications.

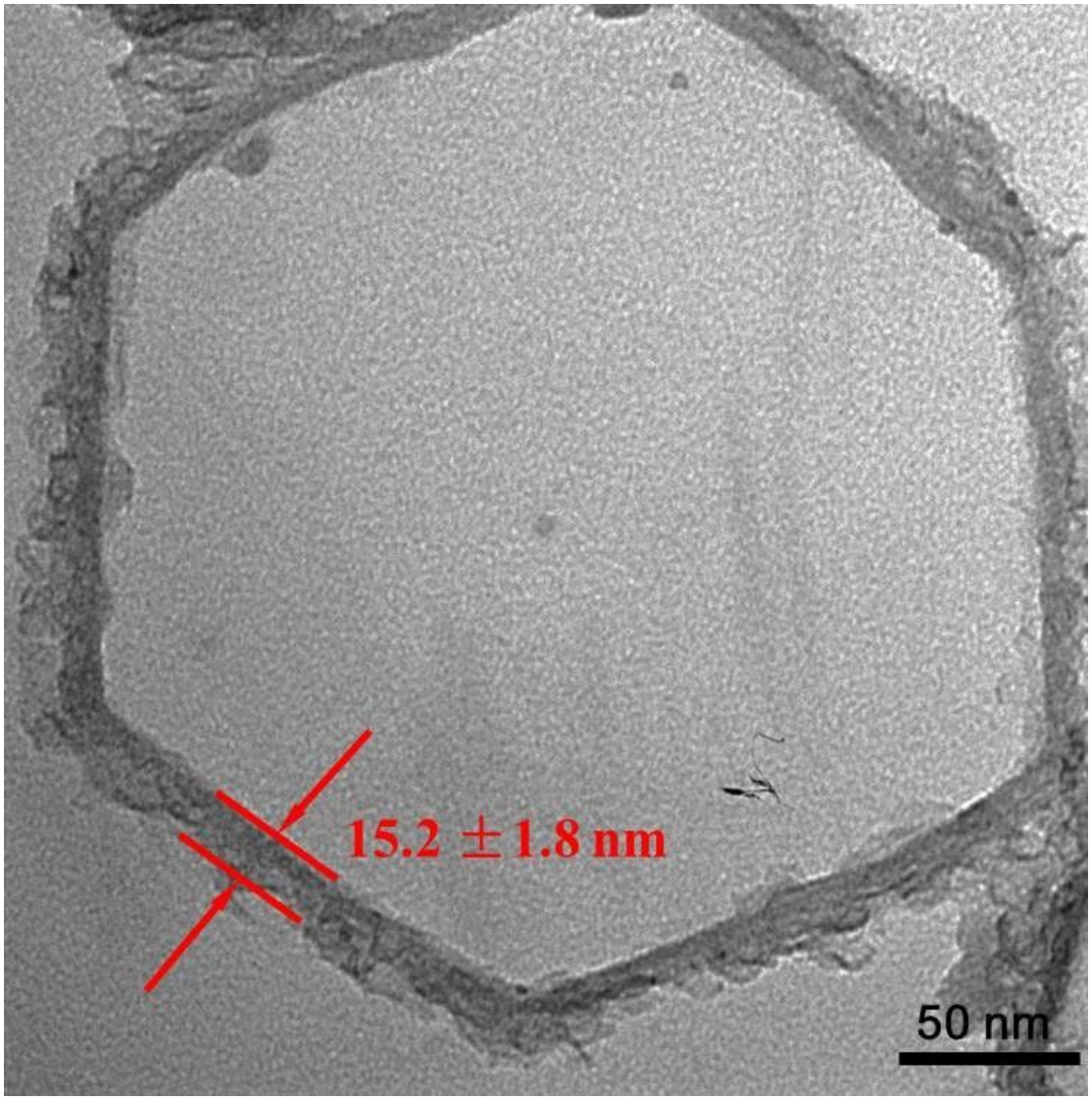

Figure S6. Representative TEM image of the single Mn doped $Cu(OH)_2$-2 mL hexagonal nanoring.

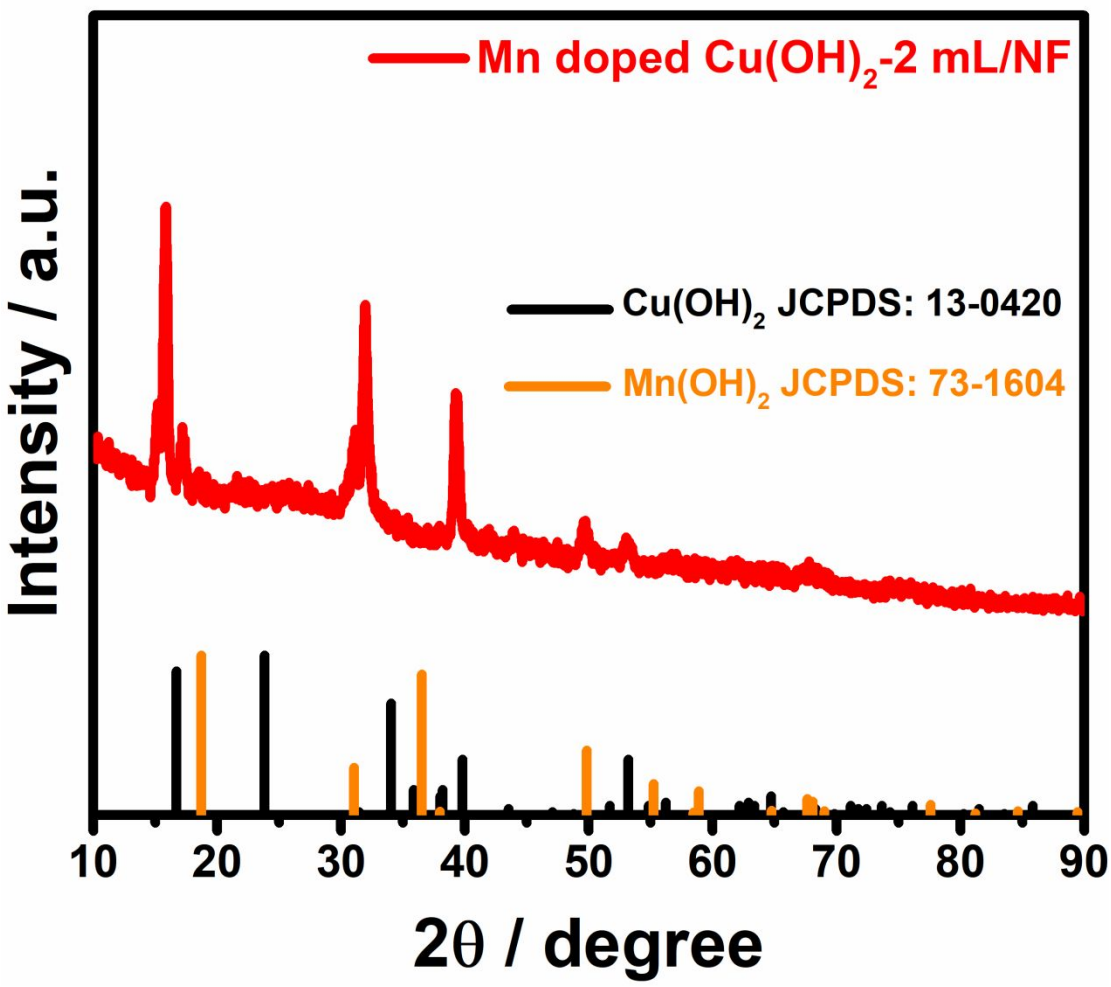

Figure S7. XRD pattern of Mn doped $Cu(OH)_2$-2 mL hexagonal nanorings.

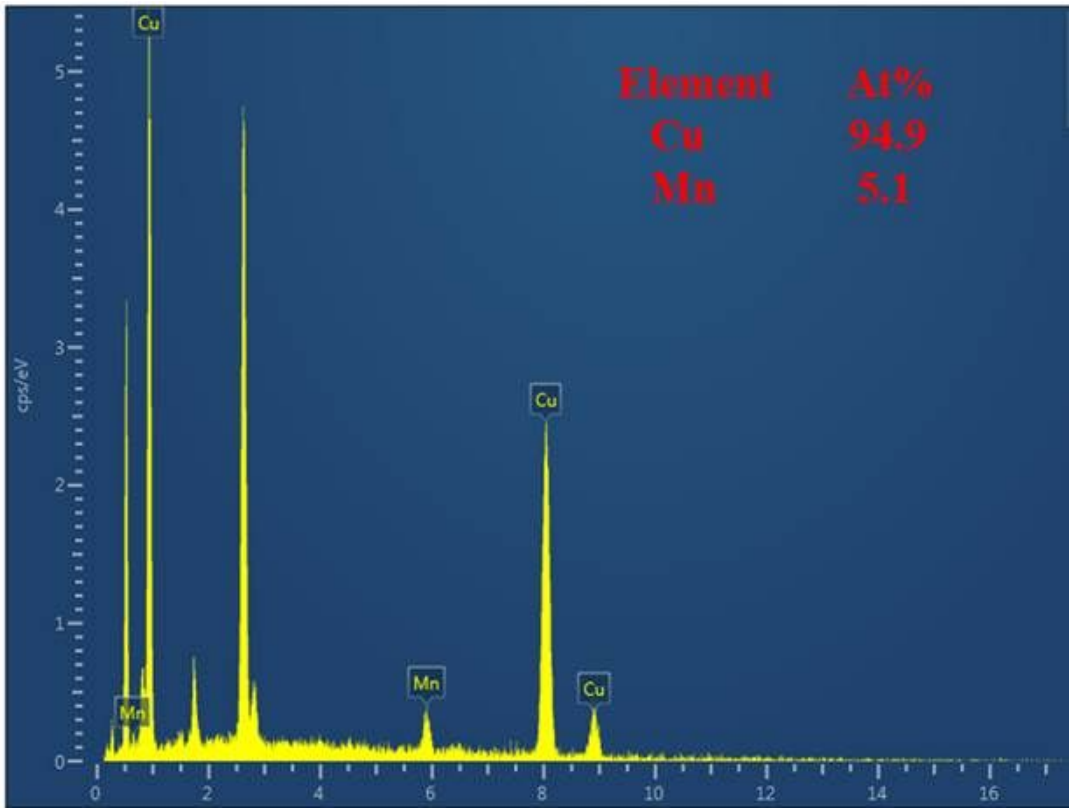

Figure S8. SEM-EDS spectrum image of Mn doped $Cu(OH)_2$-2 mL hexagonal nanorings.

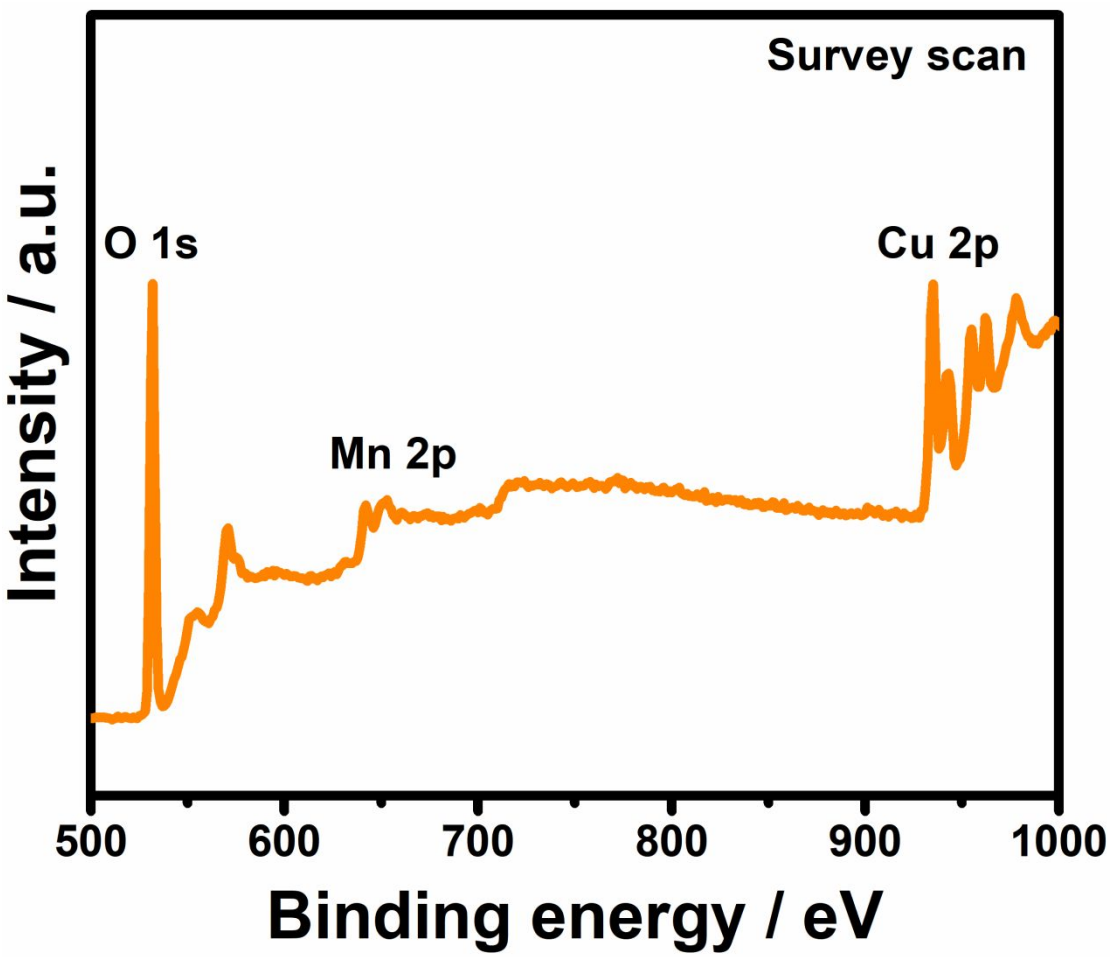

Figure S9. XPS survey spectrum of Mn doped $Cu(OH)_2$-2 mL hexagonal nanorings.

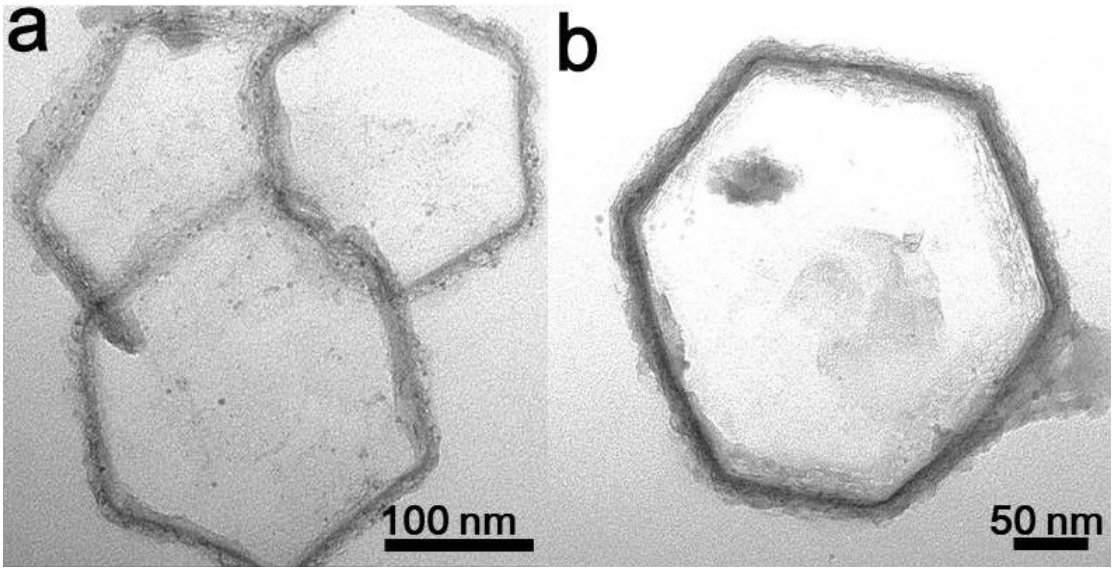

Figure S10. Representative TEM images of the (a and b) Mn doped $Cu(OH)_2$-1 mL hexagonal nanoring with different magnifications.

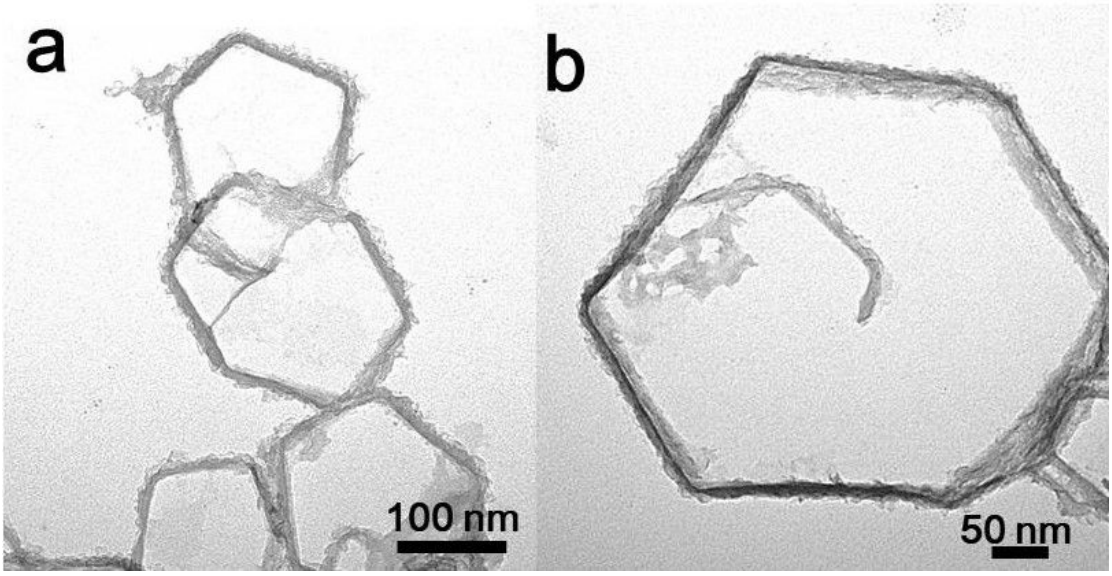

Figure S11. Representative TEM images of the (a and b) Mn doped $Cu(OH)_2$-1 mL hexagonal nanoring with different magnifications.

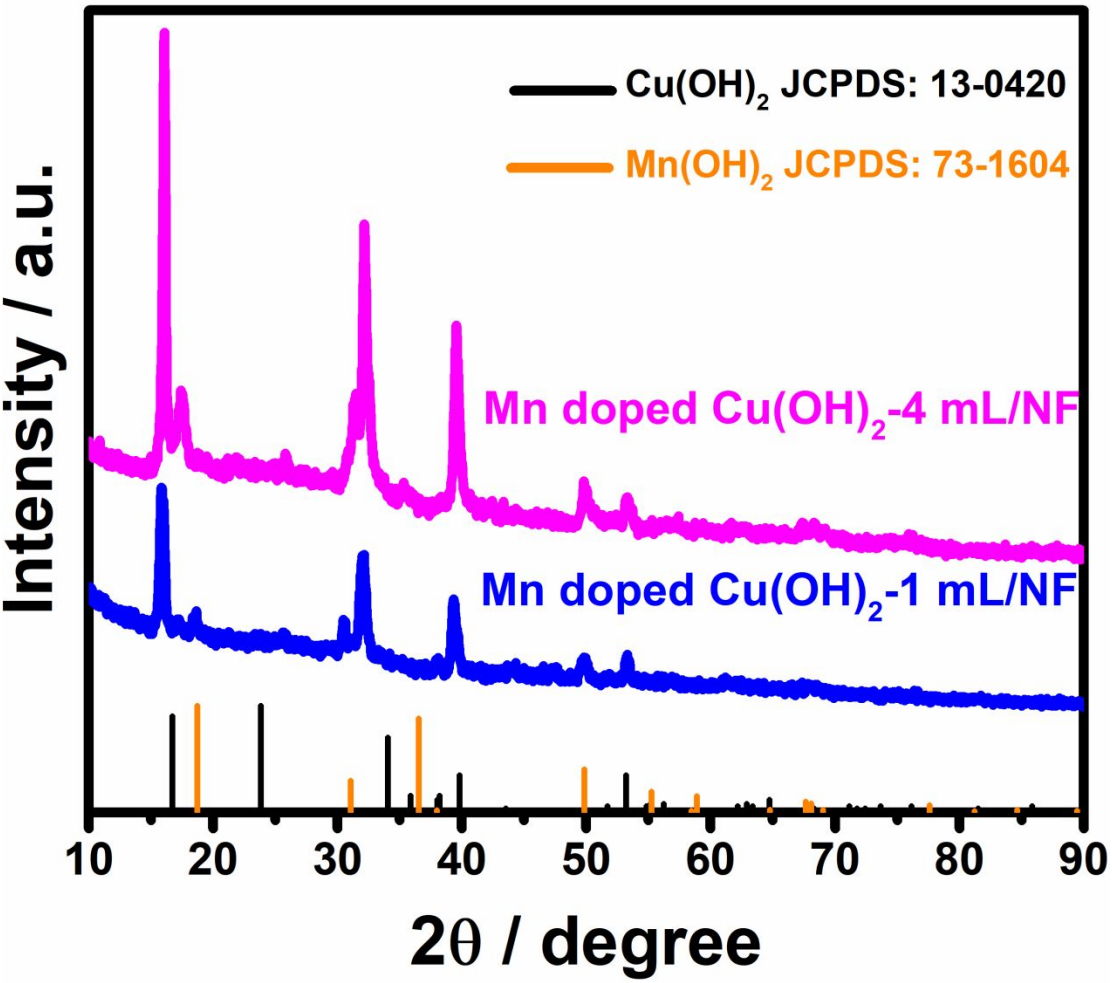

Figure S12. XRD patterns of Mn doped $Cu(OH)_2$-1 mL and Mn doped $Cu(OH)_2$-4 mL hexagonal nanorings.

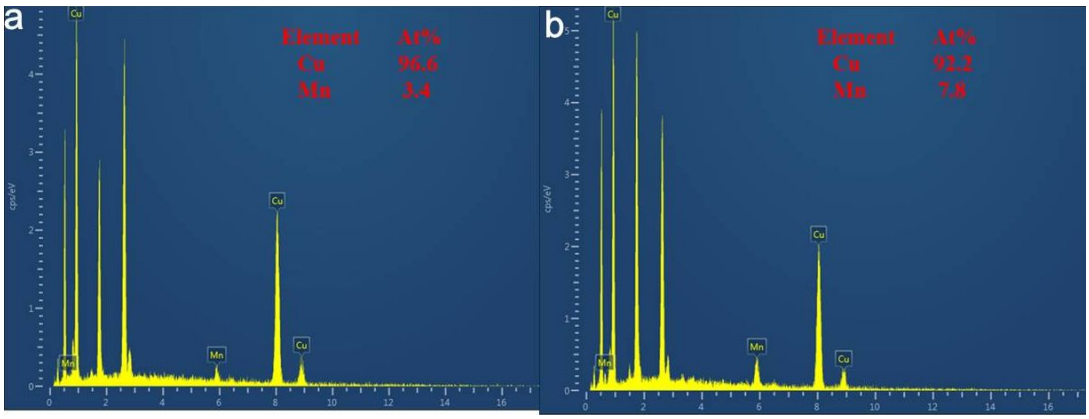

Figure S13. SEM-EDS spectrum images of (a) Mn doped $Cu(OH)_2$-1 mL and (b) Mn doped $Cu(OH)_2$-4 mL hexagonal nanorings.

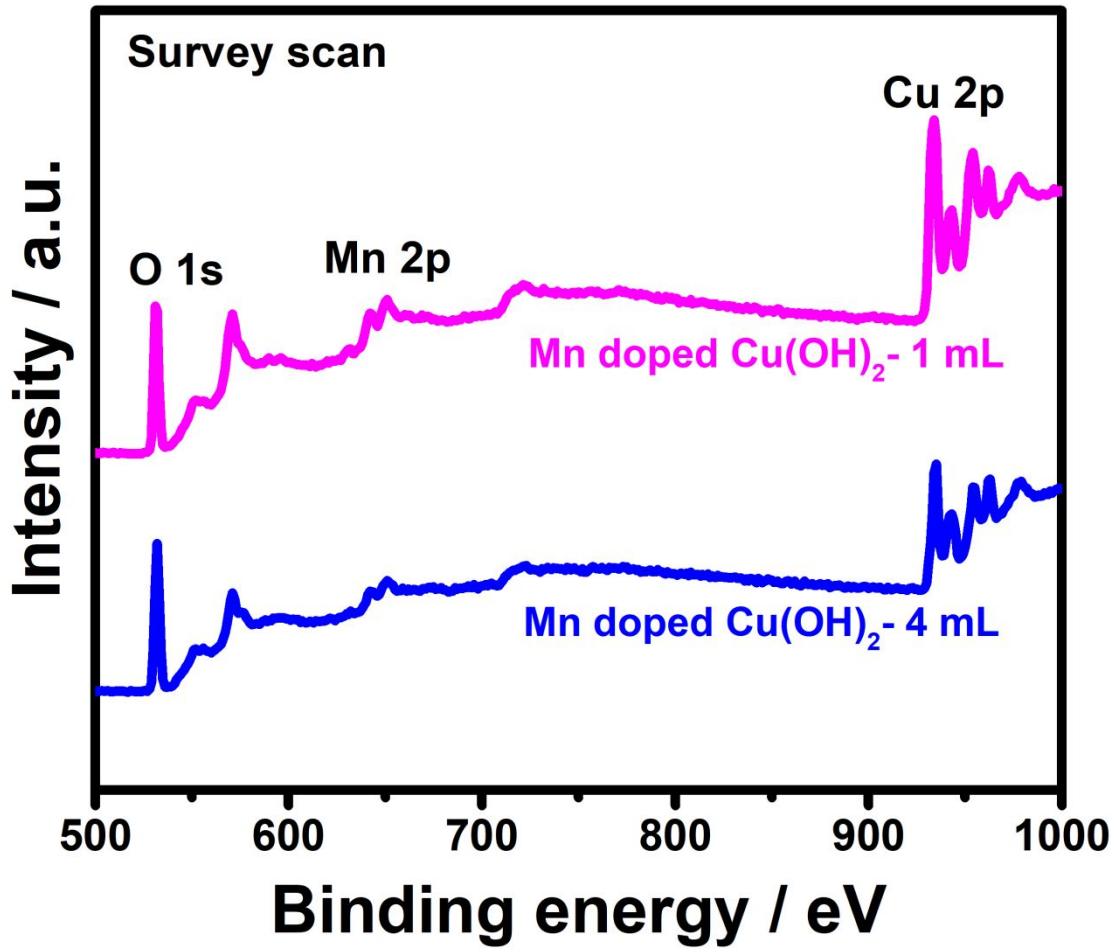

Figure S14. XPS survey spectra of Mn doped $Cu(OH)_2$-1 mL and Mn doped $Cu(OH)_2$-4 mL hexagonal nanorings.

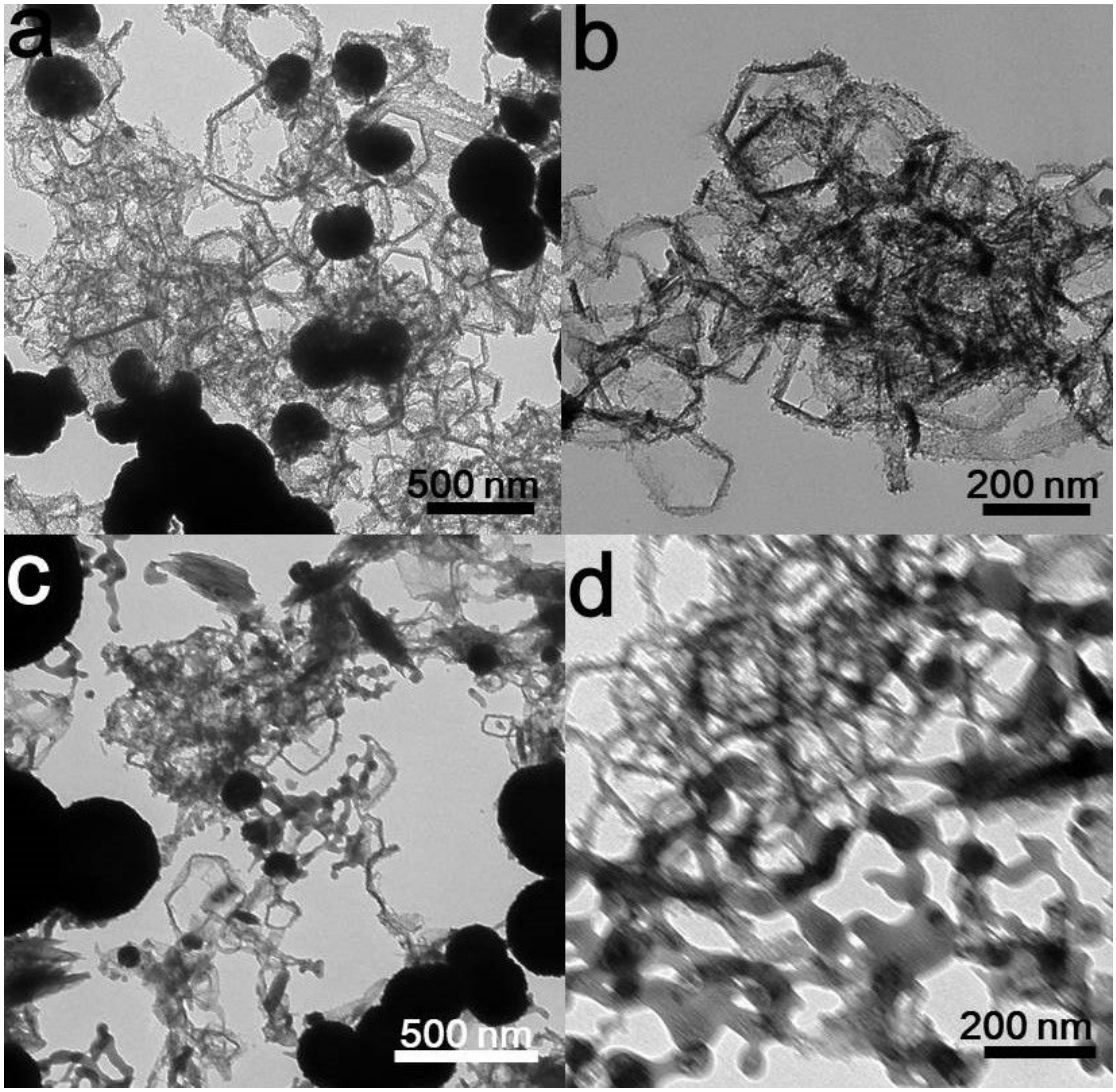

Figure S15. Representative TEM images of CuMn hydroxides prepared by replacing $CuCl_2 \cdot 2H_2O$ with (a and b) $CuSO_4$ and (c and d) $CuNO_3$, while keeping other reaction conditions remain the same. .

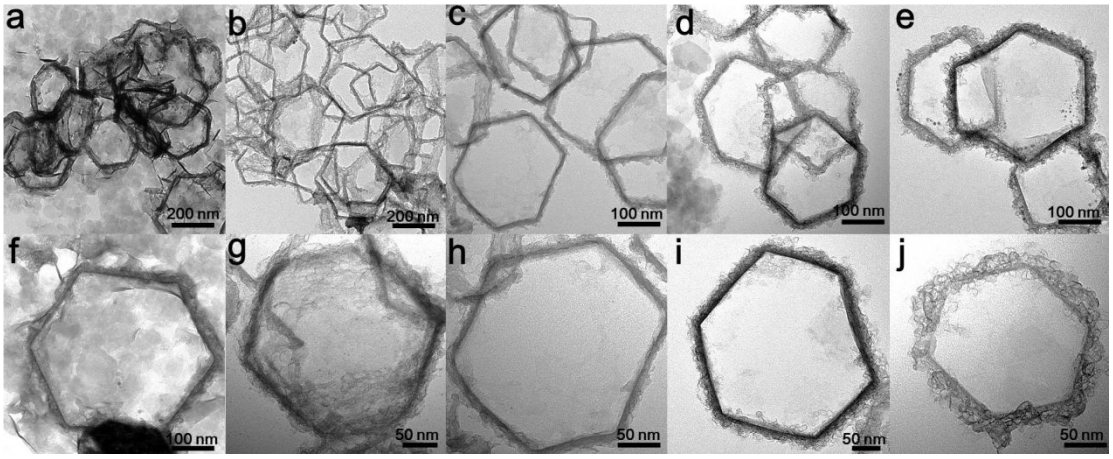

Figure S16. Representative TEM images of the intermediates of Mn doped $Cu(OH)_2$-2 mL hexagonal nanoring with the reaction times of (a and f) 3 h, (b and g) 6 h, (c and h) 12 h, (d and i)18 h, and (e and j) 24 h.

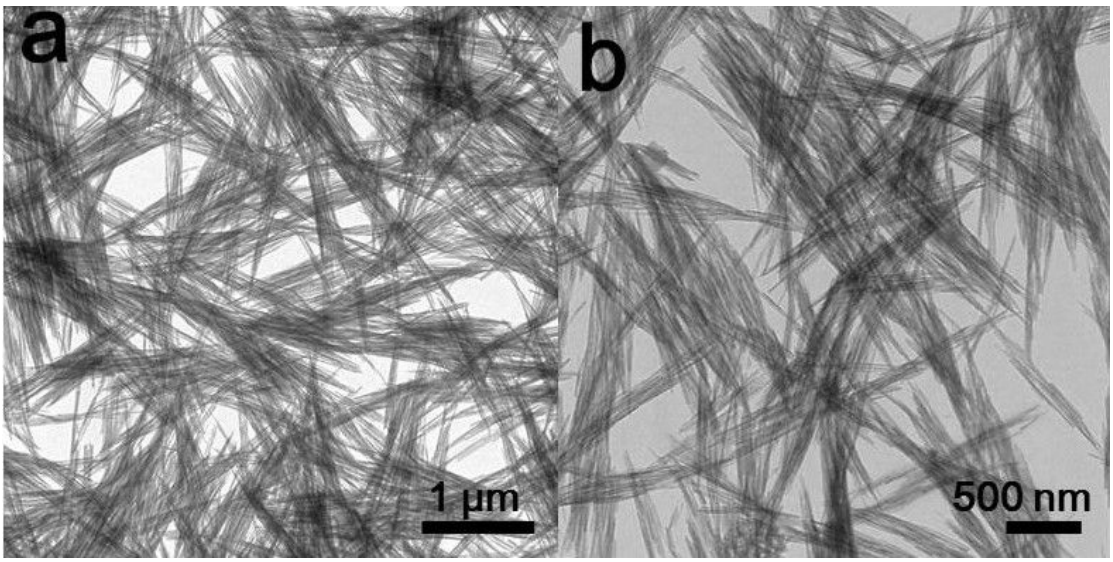

Figure S17. Representative TEM images of $Cu(OH)_2$ nanowires.

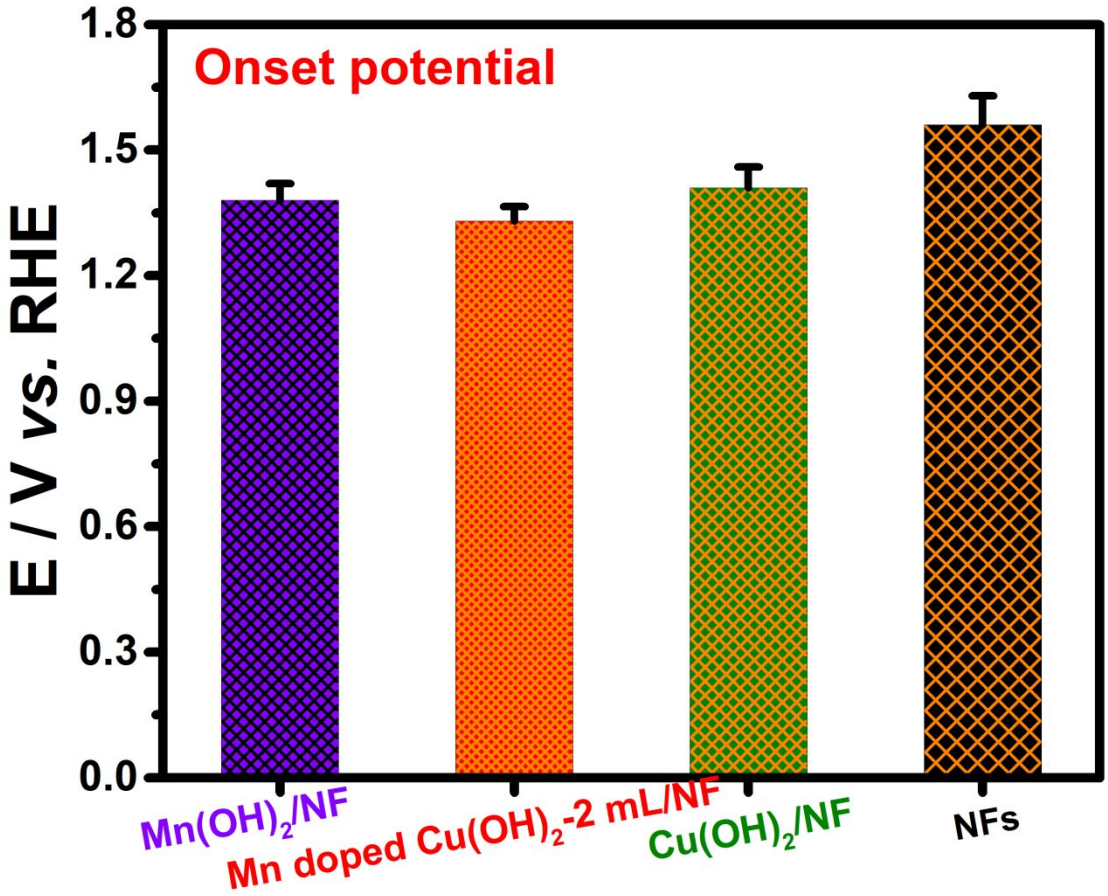

Figure S18. The onset potentials of different electrocatalysts.

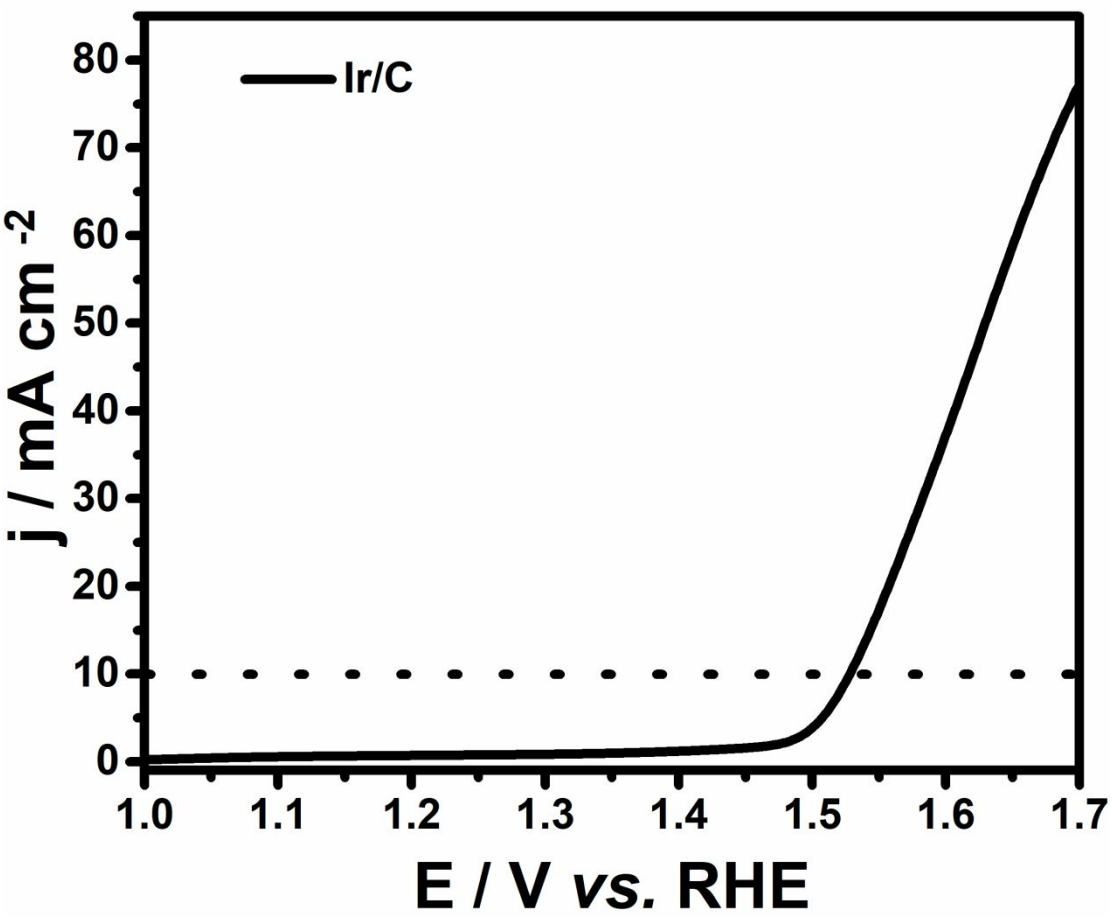

Figure S19. LSV polarization curve of commercial Ir/C catalyst in 1 M KOH solution at the scan rate of 5 mV s^{-1}.

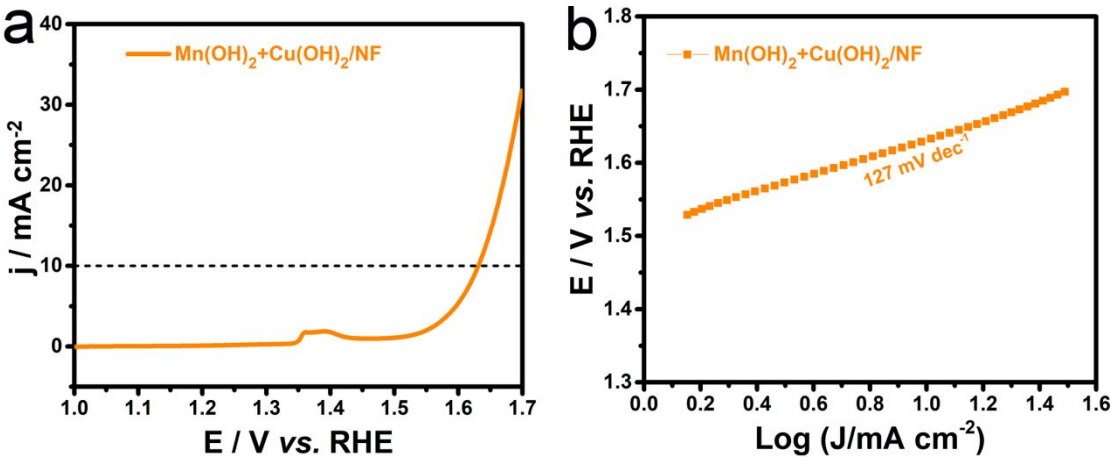

Figure S20. LSV polarization curve and tafel slope of $Cu(OH)_2$ + $Mn(OH)_2$/NF in 1 M KOH solution at the scan rate of 5 mV s^{-1}.

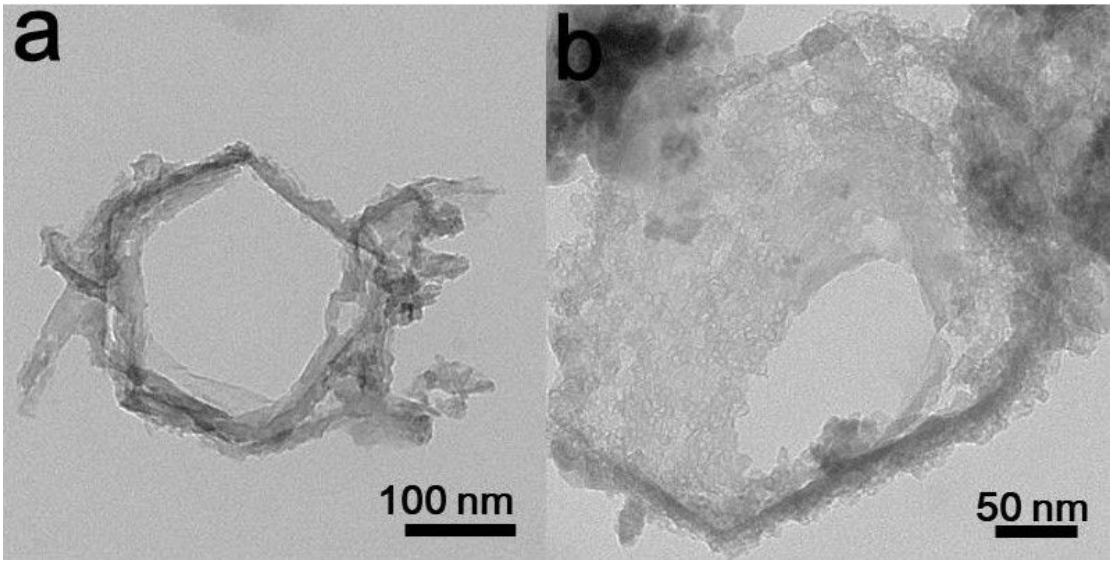

Figure S21. Representative TEM images of the Mn doped $Cu(OH)_2$-2 mL hexagonal nanoring after long-term electrochemical measurements.

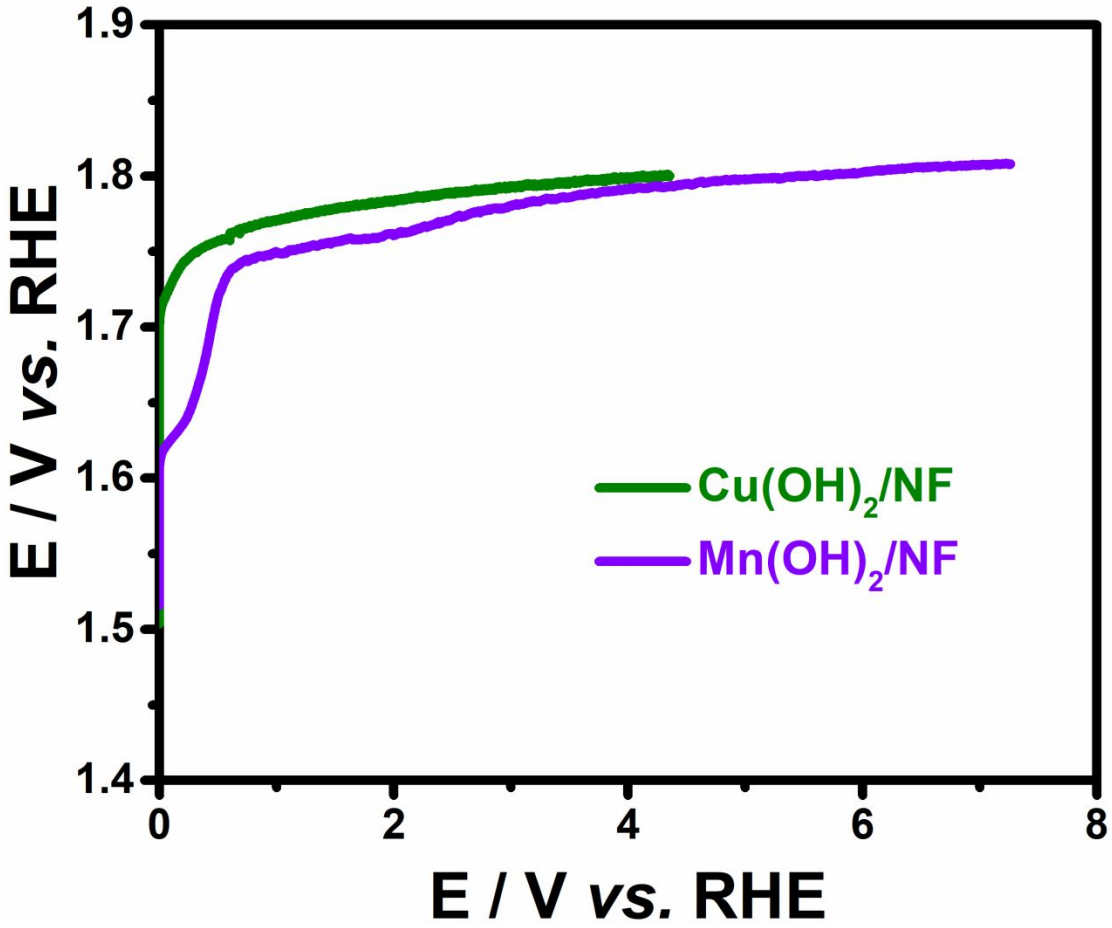

Figure S22. CP of $Cu(OH)_2$ /NF and $Mn(OH)_2$ /NF at 10 mA cm^{-2}.

.

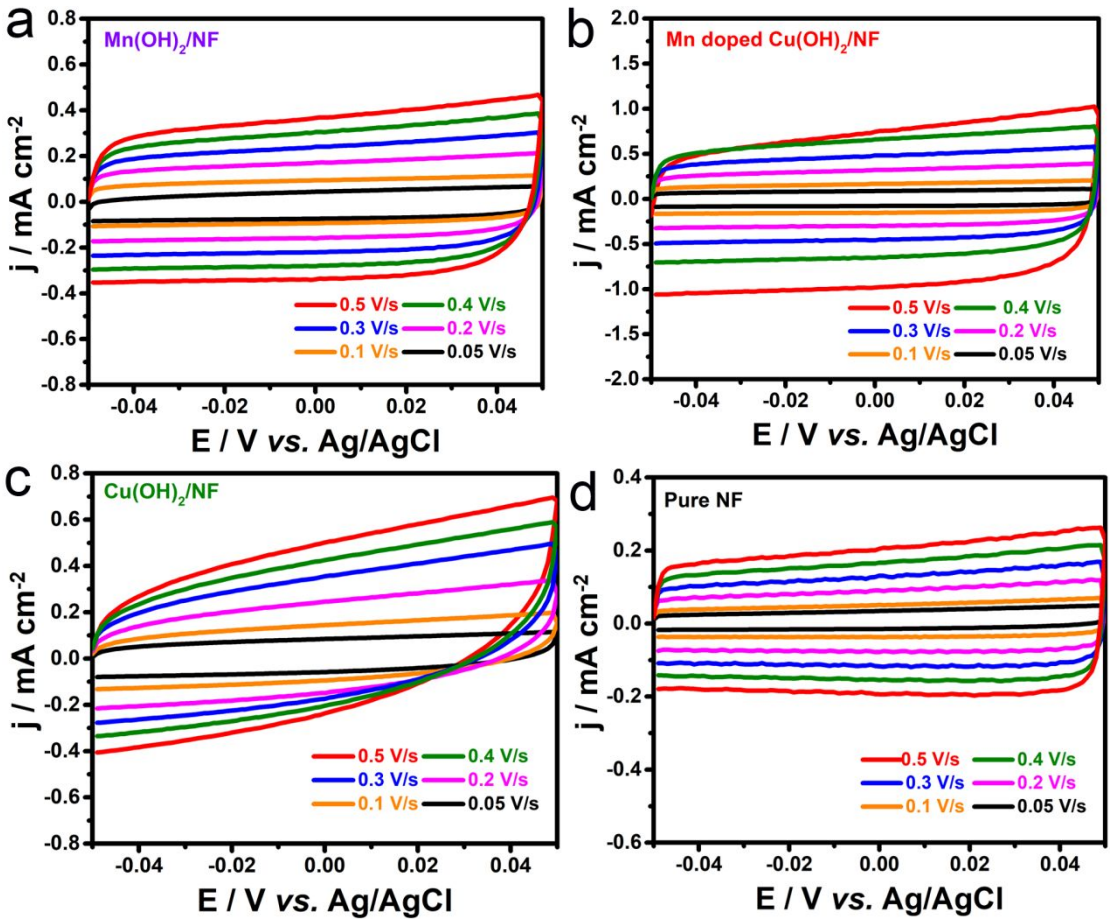

Figure S23. CV curves of (a) $Mn(OH)_2$/NF, (b) Mn doped $Cu(OH)_2$-2 mL/NF, (c) $Cu(OH)_2$/NF, and (d) NF.

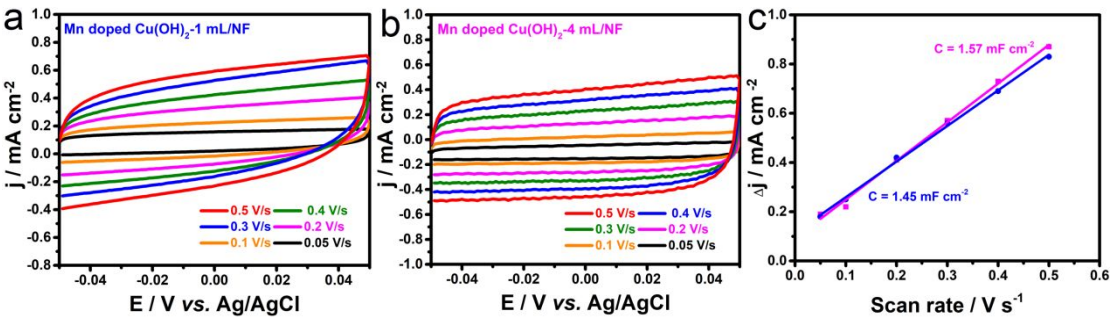

Figure S24. CV curves of (a) Mn doped $Cu(OH)_2$-1 mL and (b) Mn doped $Cu(OH)_2$-4 mL/NF. (c) Double layer currents of Mn doped $Cu(OH)_2$-1 mL and Mn doped $Cu(OH)_2$-4 mL/NF vs scan rates plots.

Table S1 Comparisons of OER activity for Mn-based electrocatalysts in alkaline condition (η: overpotential at the current density of 10 mA cm^{-2}).

Catalyst	η(mV)	Electrolyte	Reference
Mn doped $Cu(OH)_2$ HNs	**282**	1.0 M KOH	**This work**
MnO	580	0.1 M KOH	Chem. Commun. 2015, 51, 5951
MCO@PPy	560	1.0 M KOH	Electrochim. Acta 2015, 180, 788
MnO_x nanowire	>350	0.1 M KOH	Int. J. Hydrogen Energy 2017, 42,7157
α-MnO_2/MIL-101(Cr)-40	>470	1.0 M KOH	Catal. Commun. 2014, 54, 17
MnO_2/CFP	390	1.0 M KOH	Adv. Funct. Mater. 2017, 27, 1704083
$NiCoMnO_4$/NG	>430	1.0 M KOH	Appl. Mater. Environ. 2017, 201, 241-252
CoMn LDH	324	1.0 M KOH	J. Am. Chem. Soc. 2014, 136, 16481
CDs-MnO_2	343	1.0 M KOH	Carbon 2019, 143, 457

Table S2 Comparisons of OER activity for Cu-based electrocatalysts in alkaline condition (η: overpotential at the current density of 10 mA cm^{-2}).

Catalyst	η(mV)	Electrolyte	Reference
Mn doped $Cu(OH)_2$ HNs	**282**	1.0 M KOH	**This work**
Cu@NiFe LDHs	310	1.0 M KOH	Energy Environ. Sci. 2017, 10, 1820
Cu/($Cu(OH)_2$-CuO) NA/CF	350	0.1 M KOH	Electrochim. Acta 2015, 163, 102
$Cu(OH)_2$-NWAs/Cu	560	0.1 M NaOH	ChemSusChem 2016, 9, 2069
CuO NPs	290	1 M NaOH	Angew. Chem 2017, 56, 4792
Cu_2Se–Cu_2O/TF	465	1.0 M KOH	Chem. Commun 2018, 54, 4979
CuO nanowires	500	1.0 M Na_2CO_3	Nano Res. 2018, 11, 4323
CuO	420	1.0 M KOH	Electrochim. Acta 2018, 263, 318
Cu_2O	420	1.0 M KOH	Electrochim. Acta 2016, 187, 381
MWCNT/CuO	420	1.0 M KOH	J. Alloy Compds 2018, 735, 2311

Table S3 Comparisons of OER activity for Co/Ni/Fe-based electrocatalysts in alkaline condition (η: overpotential at the current density of 10 mA cm^{-2}).

Catalyst	η(mV)	Electrolyte	Reference
Mn doped $Cu(OH)_2$ HNs	**282**	1.0 M KOH	**This work**
$Ir_{0.46}Co_{0.54}O_y$ nanotubes	310	1.0 M KOH	ACS Appl. Mater. Interface, 2017, 9, 35057
Ni_3Se_4	320	1.0 M KOH	Nanoscale 2018, 10, 5163
CoO_x-ZIF	318	1.0 M KOH	Adv. Funct. Mater. 2017, 1702546
Co_3O_4@CoO SC	430	1.0 M KOH	Nat. Commun. 2015, 6, 8
$CoSe_2$/N-doped graphene	366	0.1 M KOH	ACS Nano 2014, 8, 3970
ZnCo LDH	>330	1.0 M KOH	J. Mater. Chem. A, 2014, 2, 13250
Co@Co–Bi/Ti	327	1.0 M KOH	Nanoscale 2017, 9, 16059
Fe_3O_4 cubes	336	1.0 M KOH	ACS Energy Lett. 2018, 3, 861-868
Ni_5P_4	470	1.0 M KOH	Angew. Chem. Int. Ed. 2015, 54, 12361
CoO_x-ZIF	318	1.0 M KOH	Adv. Funct. Mater. 2017, 1702546
Ni-Co oxides layers	325	1.0 M KOH	ACS Nano 2014, 8, 9518
Au@Co_3O_4	378	1.0 M KOH	Adv. Mater. 2014, 26, 3950
Co_3O_4@CoO SC	430	1.0 M KOH	Nat. Commun. 2015, 6, 8.
Ni-Co oxides layers	325	1.0 M KOH	ACS Nano 2014, 8, 9518

Reference:

1. X. Zhang, Z. Xing, L. L. Wang, Y. C. Zhu, Q. W. Li, J. W. Liang, Y. Yu, T. Huang, K. B. Tang, Y. T. Qian, X. Y. Shen, *J. Mater. Chem.* **2012**, 22, 17864.